

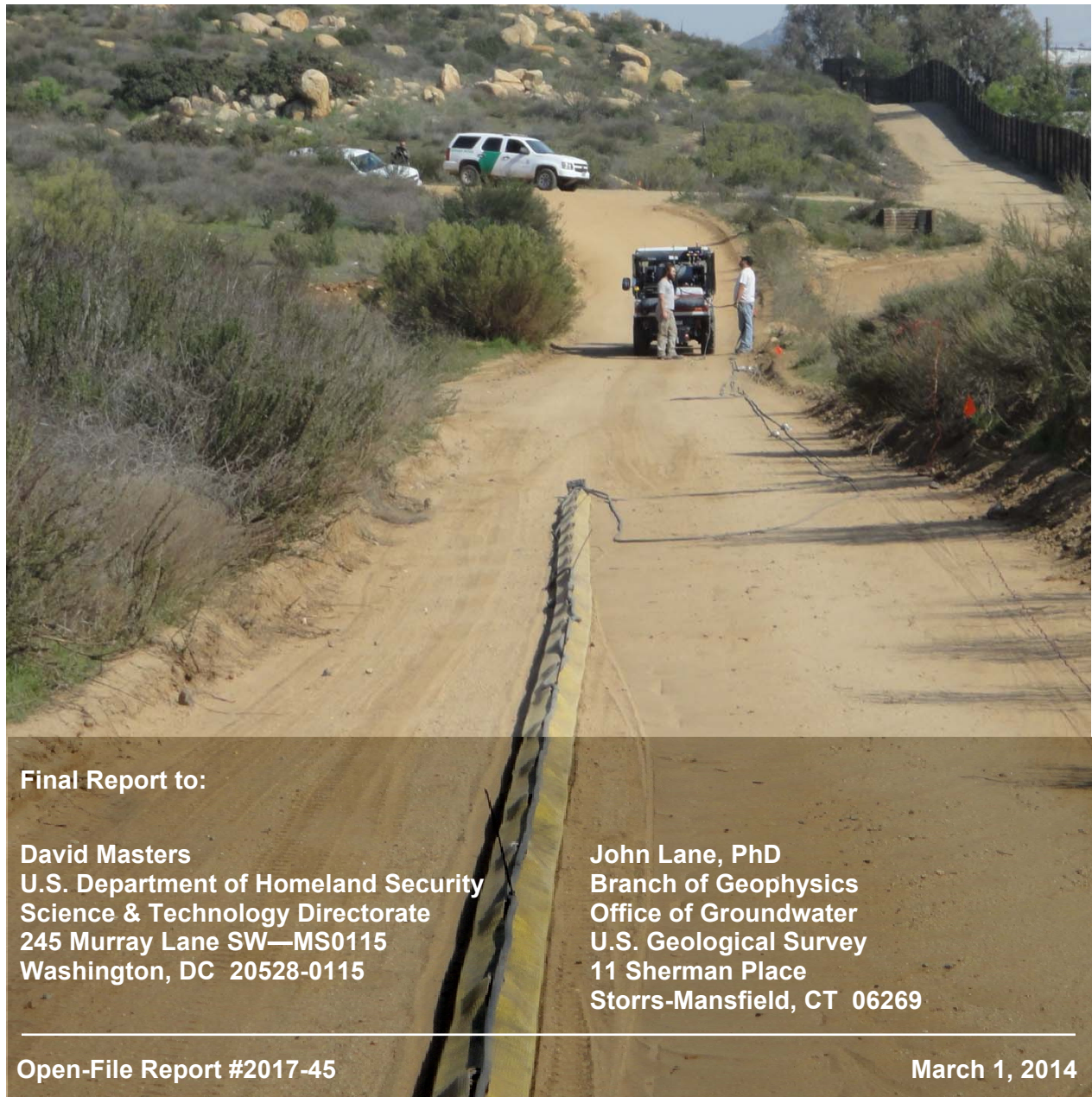
# Final Report: Seismic Analysis at Strategic Border Sites

## DTRA-T1

---

Richard D. Miller, Julian Ivanov, Shelby L. Peterie,  
J. Tyler Schwenk, Brett E. Judy, J. Jordan Nolan,  
Brett Wedel, Ryan Nelson, Brett Bennett, and Joe Anderson

Kansas Geological Survey  
1930 Constant Avenue  
Lawrence, KS 66047



**Final Report to:**

David Masters  
U.S. Department of Homeland Security  
Science & Technology Directorate  
245 Murray Lane SW—MS0115  
Washington, DC 20528-0115

John Lane, PhD  
Branch of Geophysics  
Office of Groundwater  
U.S. Geological Survey  
11 Sherman Place  
Storrs-Mansfield, CT 06269

The Kansas Geological Survey makes no warranty or representation, either express or implied, with regard to the data, documentation, or interpretations or decisions based on the use of this data including the quality, performance, merchantability, or fitness for a particular purpose. Under no circumstances shall the Kansas Geological Survey be liable for damages of any kind, including direct, indirect, special, incidental, punitive, or consequential damages in connection with or arising out of the existence, furnishing, failure to furnish, or use of or inability to use any of the database or documentation whether as a result of contract, negligence, strict liability, or otherwise. This study was conducted in complete compliance with ASTM Guide D7128-05. All data, interpretations, and opinions expressed or implied in this report and associated study are reasonably accurate and in accordance with generally accepted scientific standards.

# **Final Report: Seismic Analysis at Strategic Border Sites DTRA-T1**

## **Summary**

The Kansas Geological Survey acquired borehole and surface seismic data at 15 DHS sites near the US-Mexico border. Surface seismic data were processed using multi-channel analysis of surface waves (MASW), refraction tomography, and surface wave inversion to obtain 2-D profiles of shear-wave velocity ( $V_s$ ), compressional-wave velocity ( $V_p$ ), and seismic quality factor ( $Q_s$  and  $Q_p$ ) for the near surface. Downhole data were processed to obtain downhole  $V_s$ ,  $V_p$ ,  $Q_s$ , and  $Q_p$ . This report contains final processing and results for DTRA-T1.

## **Data Acquisition**

Two lines of seismic data were acquired on February 18, 2013, at DTRA-T1 coincident with the USGS ERT profiles (Figure 1). Lines 1000 and 2000 were approximately 285 m and 170 m long, respectively. The system of sources and receivers, collectively, is the Active Seismic Imaging (ASI) system developed by and fabricated at the Kansas Geological Survey (Figure 2). Seismic sources were an accelerated weight drop for surface wave and long-offset compressional energy, sledge hammer and steel plate for near-offset compressional-wave energy, and sledge hammer and shear block for shear-wave energy. Seismic receivers were located in a towed 144-channel 3-component (3-C) land streamer with 48 stations separated by 1.2 m. Receivers were single 4.5 Hz and 40 Hz vertical geophones and two 14.5 Hz horizontal (SV orientation) geophones (Figure 3). Seismographs were a Geometrics Geode distributed system. The survey was fixed spread with variable 0-85.3 m source offset (Figure 4) to obtain sufficient seismic sampling within the depth of interest. Individual receiver spreads overlapped by one station.

Downhole data were acquired on January 26, 2014, near the west end of line 1000, with a 3-C downhole Geostuff geophone (Figure 5). Receivers were located between depths of approximately 1.5 m and 18.3 m at approximately 0.75 m intervals (Figure 6). A repeatable shear and compressional 9 kg hammer source (Figure 7), developed and fabricated at the Kansas Geological Survey, was located at 3 m from the borehole. A 2.7 kg sledge hammer and steel plate were located at 22.9 m from the borehole.

For both the surface and downhole seismic surveys, multiple shots were acquired and recorded separately for each unique shot/receiver configuration and stacked during processing to minimize ambient noise (Figure 8) and increase the signal-to-noise ratio.



**Figure 1:** Aerial photo of DTRA-T1 and locations of active seismic lines.



**Figure 2:** ASI towing a 144-channel 3-C land streamer with the shear block and sledge hammer source in use.

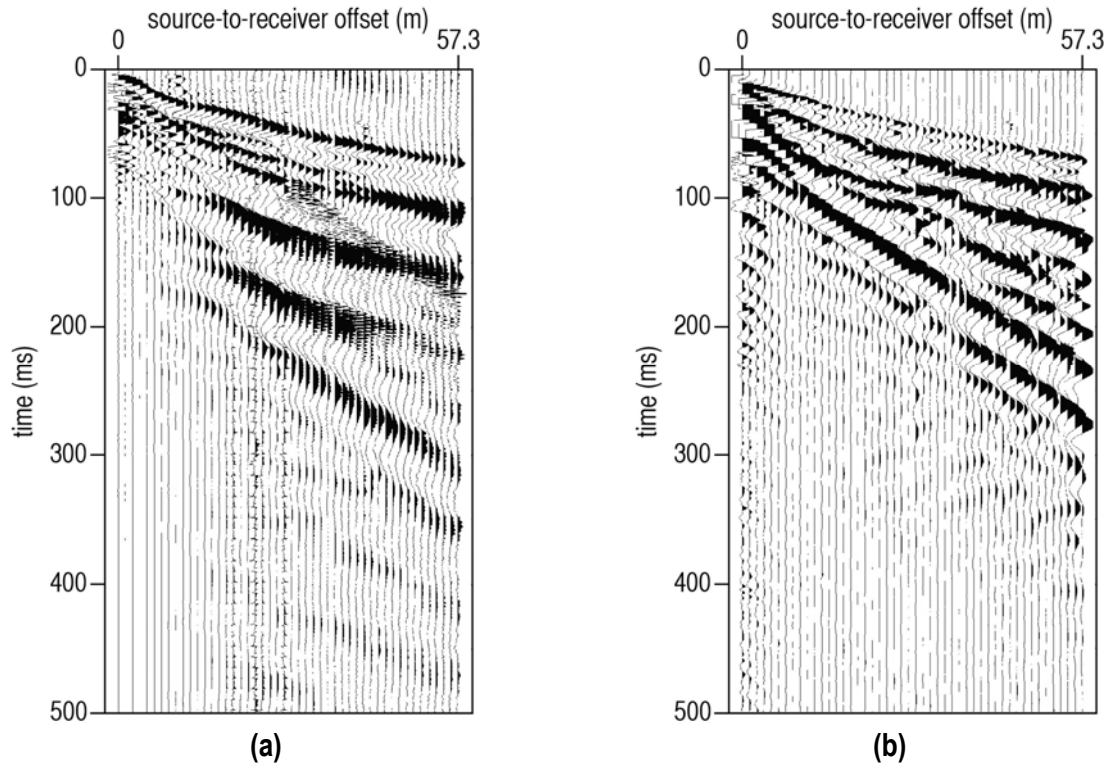


**Figure 3:** Representative off-end shot gathers at DTRA-T1. (a) Sledge hammer and shear block source recorded with shear 14.5 Hz geophones, SV orientation. (b) Weight-drop source recorded with vertical 40 Hz geophones.

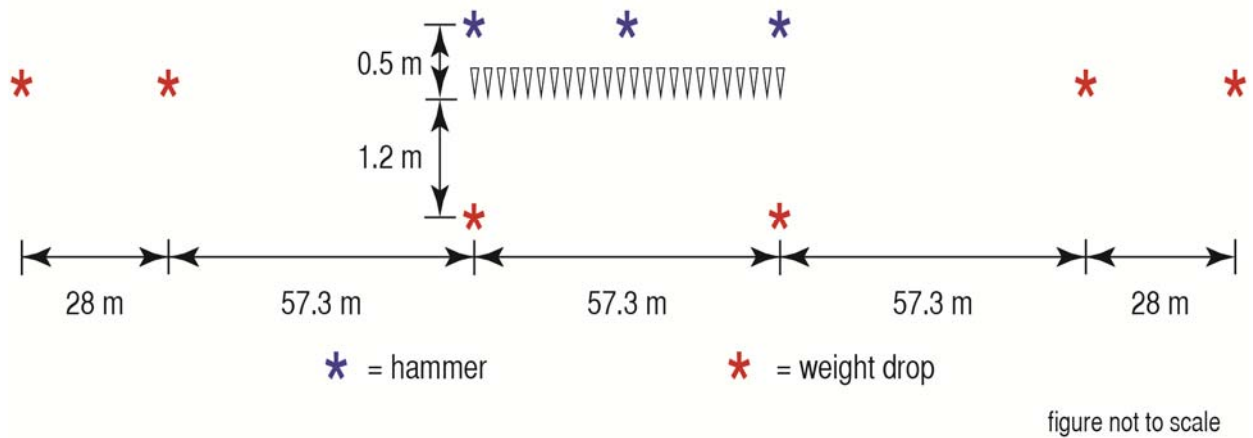


**Figure 4:** Diagram indicating all shot point locations relative to a single receiver spread. The receiver spread consisted of 48 stations separated by 1.2 m.

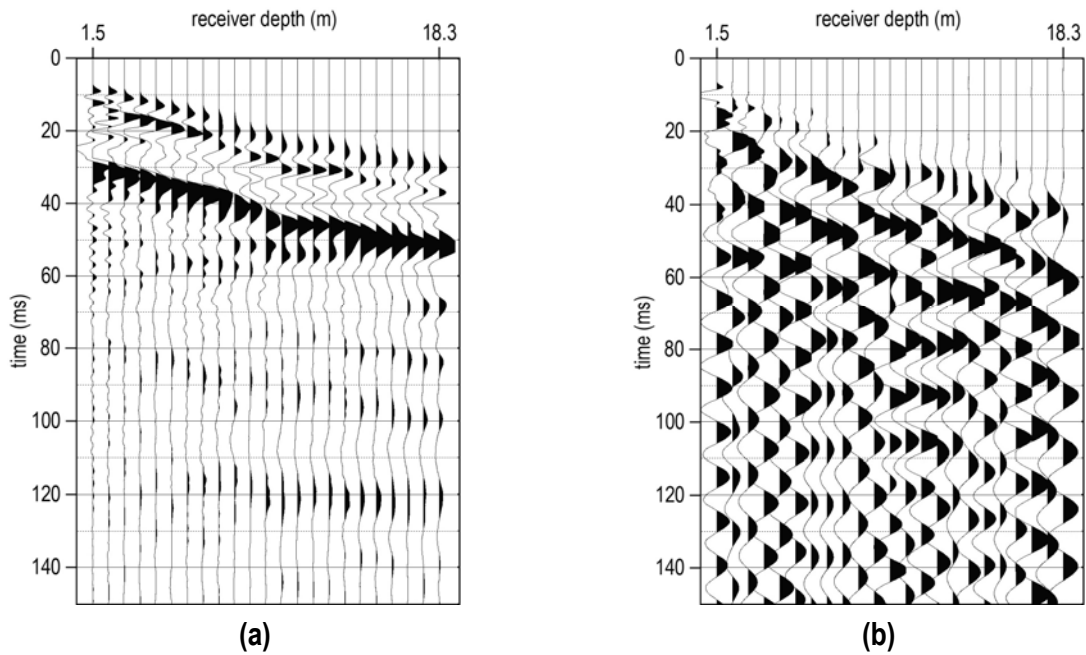


**Figure 5:** Representative unprocessed downhole (a) vertical and (b) shear records at DTRA-T1.

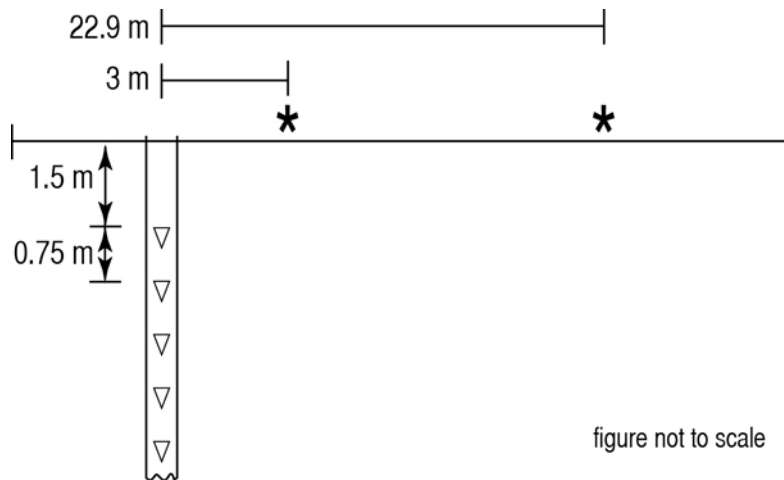


**Figure 6:** Downhole seismic field layout.



**Figure 7:** Downhole seismic acquisition at DTRA-T1.

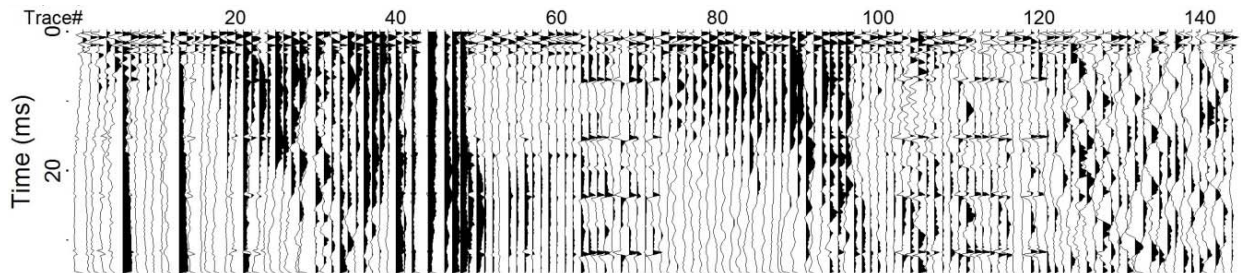


**Figure 8:** Representative ambient noise recorded at DTRA-T1. Traces 1-48 represent the 4.5 Hz geophones, 49-96 represent the shear geophones, and 97-144 represent the 40 Hz geophones.

## Data Processing

Multichannel-analysis of surface waves (MASW) was used to analyze dispersive Rayleigh-wave energy and estimate shear-wave velocity ( $V_s$ ). Fundamental-mode energy was interpreted and inverted using a weighted, damped least-squares approach (Xia et al., 1999), resulting in a 2-D  $V_s$  profile. Average and interval downhole compressional-wave velocity ( $V_p$ ) and  $V_s$  were calculated using the arrival time of the direct P-wave and S-wave, respectively, and pathlength from the seismic source to each receiver depth. Refraction tomography with 1.2 x 1.2 m cell size was used to estimate  $V_s$  and  $V_p$ . Joint-analysis of refractions and surface waves (JARS, Ivanov et al., 2010) was used to constrain the non-uniqueness inherently involved in refraction inversion, resulting in physically realistic 2-D  $V_s$  and  $V_p$  profiles. Shear- and compressional-wave seismic quality factors ( $Q_s$  and  $Q_p$ , respectively) were obtained using a surface wave inversion technique (Xia et al., 2010). Downhole shear records were numerically rotated to orient the recorded shear-wave traces in the vertical (SV) and horizontal (SH) polarization directions (Di Siena et al., 1984). The direct P-waves and S-waves were isolated on compressional and shear records, respectively, and the spectral ratio method was used to estimate  $Q_p$  and  $Q_s$  for each lithology identified in drilling notes (Tonn, 1991; Hasse and Stewart, 2004). The velocity and quality values calculated from downhole data were used to constrain inversion and improve accuracy of the results obtained using surface seismic methods.

## Final Results

### MASW

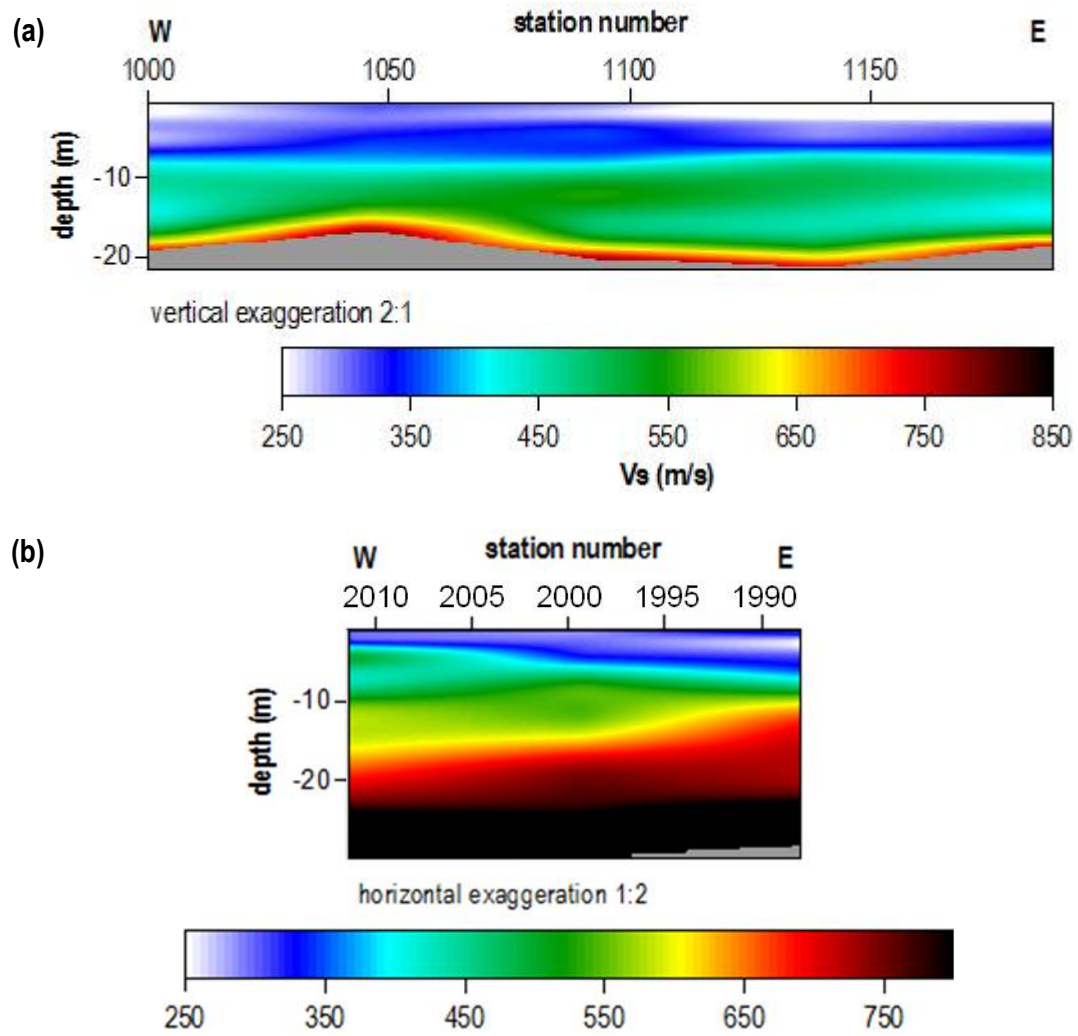


**Figure 9:** MASW Vs profiles for lines (a) 1000 and (b) 2000 at DTRA-T1. Gray represents areas with no data.

### Downhole Vs

Bond logs indicate the grout is not well bonded to the formation between receiver depths of 1.5 to 13 m. Therefore, arrival times, and thus velocity, on the traces within this interval have greater uncertainty.

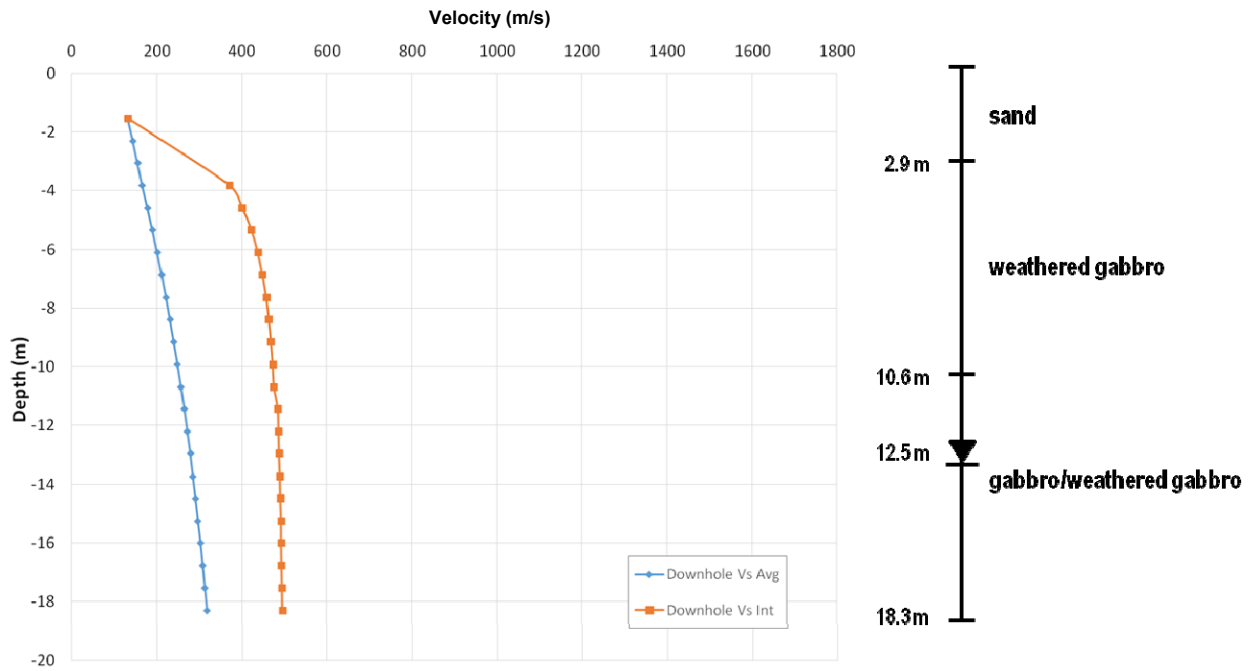


Figure 10: Downhole Vs profile at DTRA-T1.

### Downhole $V_p$

Bond logs indicate the grout is not well bonded to the formation between receiver depths of 1.5 to 13 m according to bond logs, and the waveforms of direct P-wave recorded within range is inconsistent with deeper receiver stations (Figure 5a). Arrival times, and thus velocity, on the traces within this interval have greater uncertainty.

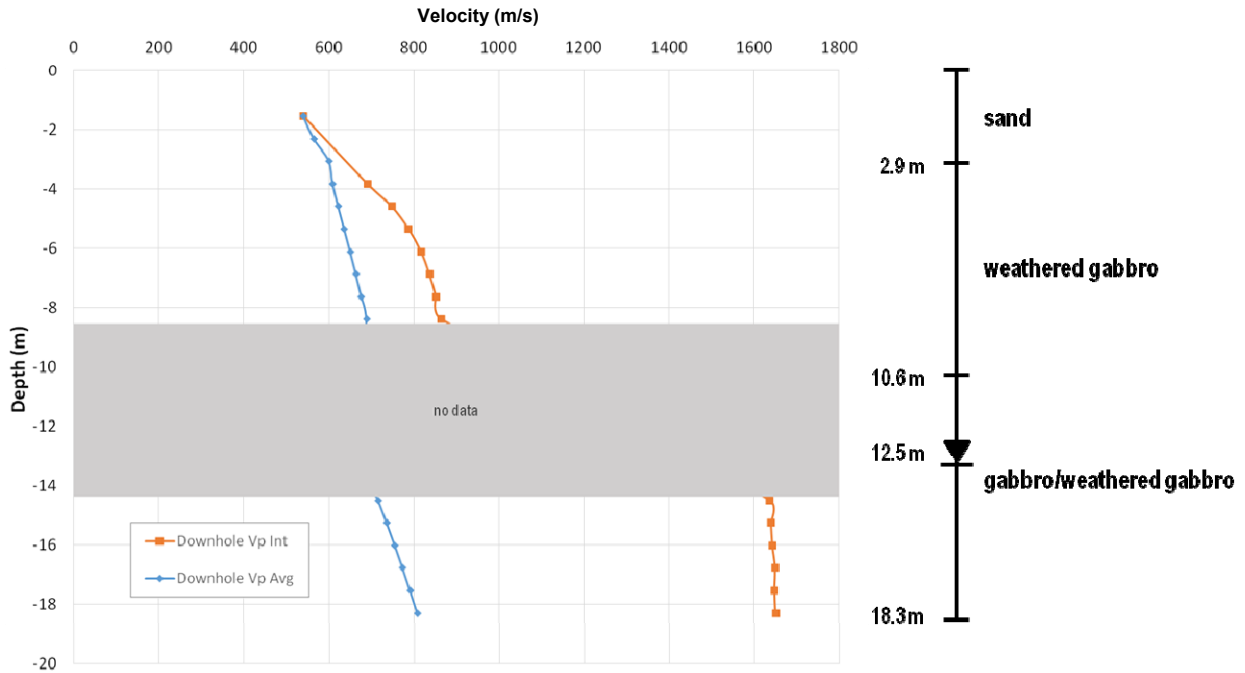
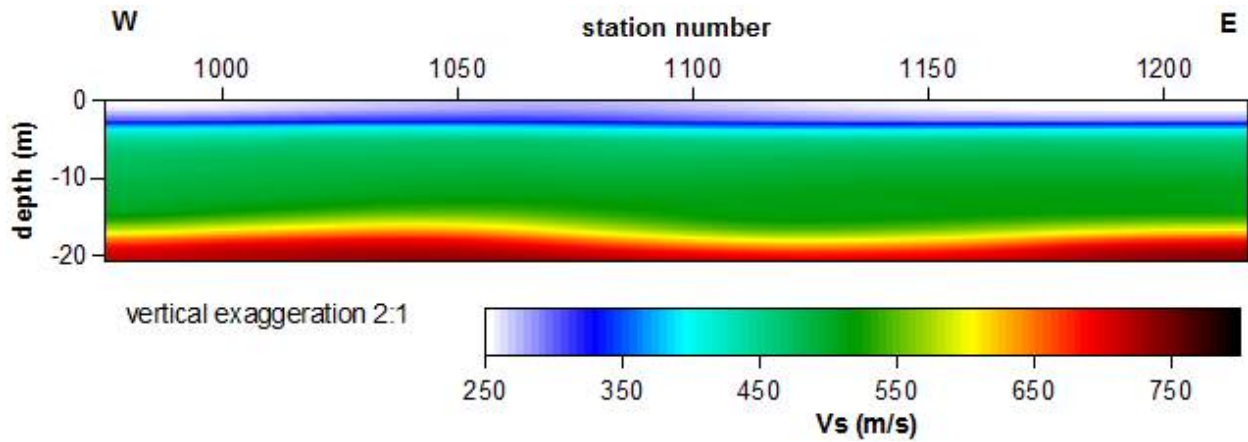


Figure 11: Downhole  $V_p$  profile at DTRA-T1.

### *Vs Tomography*

The initial model for final tomography results was generated based on downhole interval S-wave velocities. Picked first arrival times used for preliminary processing were reviewed to confirm their accuracy and used for final processing.



**Figure 12:** Vs tomography profiles for line 1000 at DTRA-T1.

### *V<sub>p</sub> Tomography*

The initial model for final tomography results on line 1000 was generated based on downhole interval P-wave velocities. A scaled, smoothed version of the final MASW V<sub>s</sub> profile was used as the initial model on line 1000. Picked first arrival times used for preliminary processing were reviewed to confirm their accuracy and used for final processing of both lines.

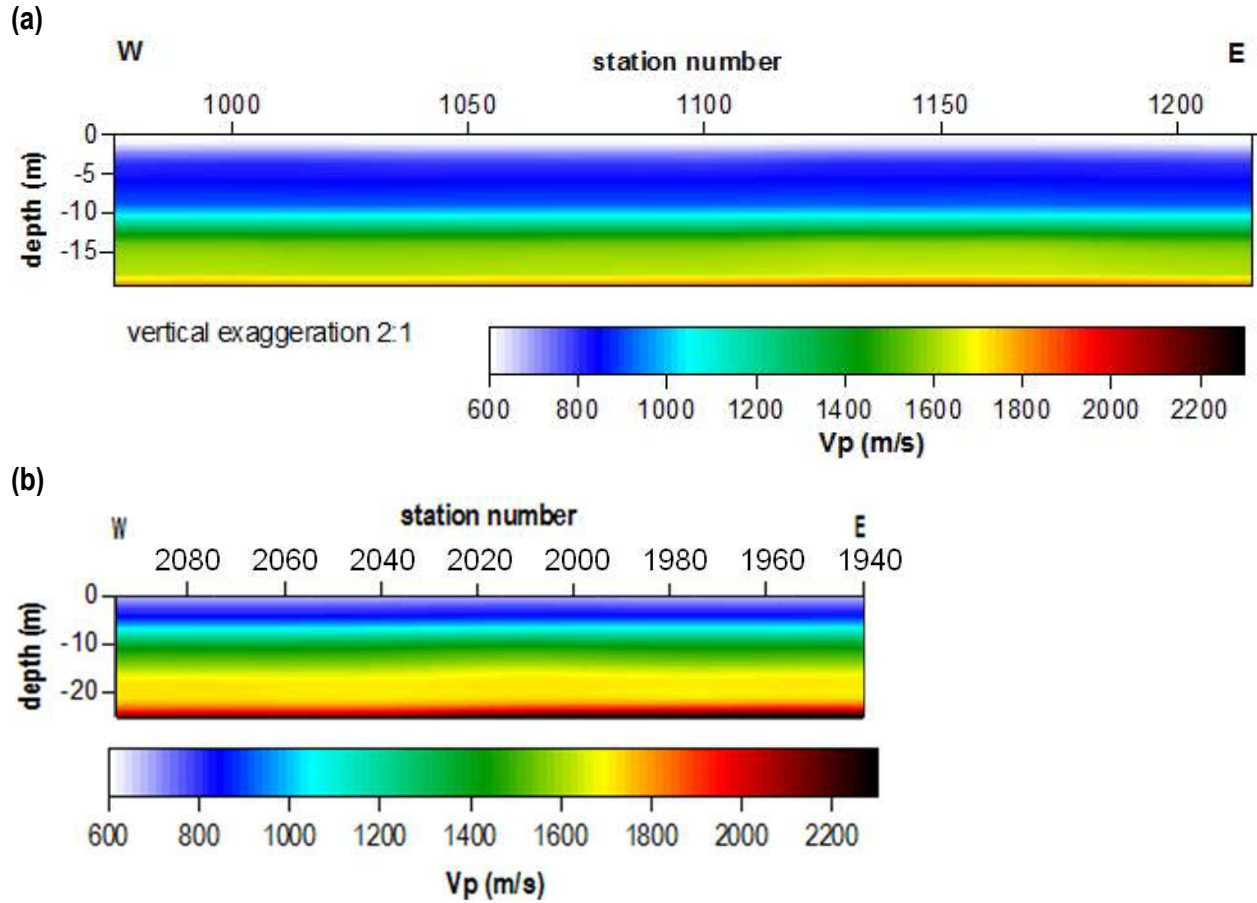


**Figure 13:** V<sub>p</sub> tomography profiles for lines (a) 1000 and (b) 2000 at DTRA-T1.

### Downhole Qs

Bond logs indicate the grout is not well bonded to the formation between receiver depths of 1.5 and 13 m. Therefore, Q estimates for traces within this interval have greater uncertainty. Calculation of Q is highly sensitive to sources of noise (e.g., traffic) during acquisition.

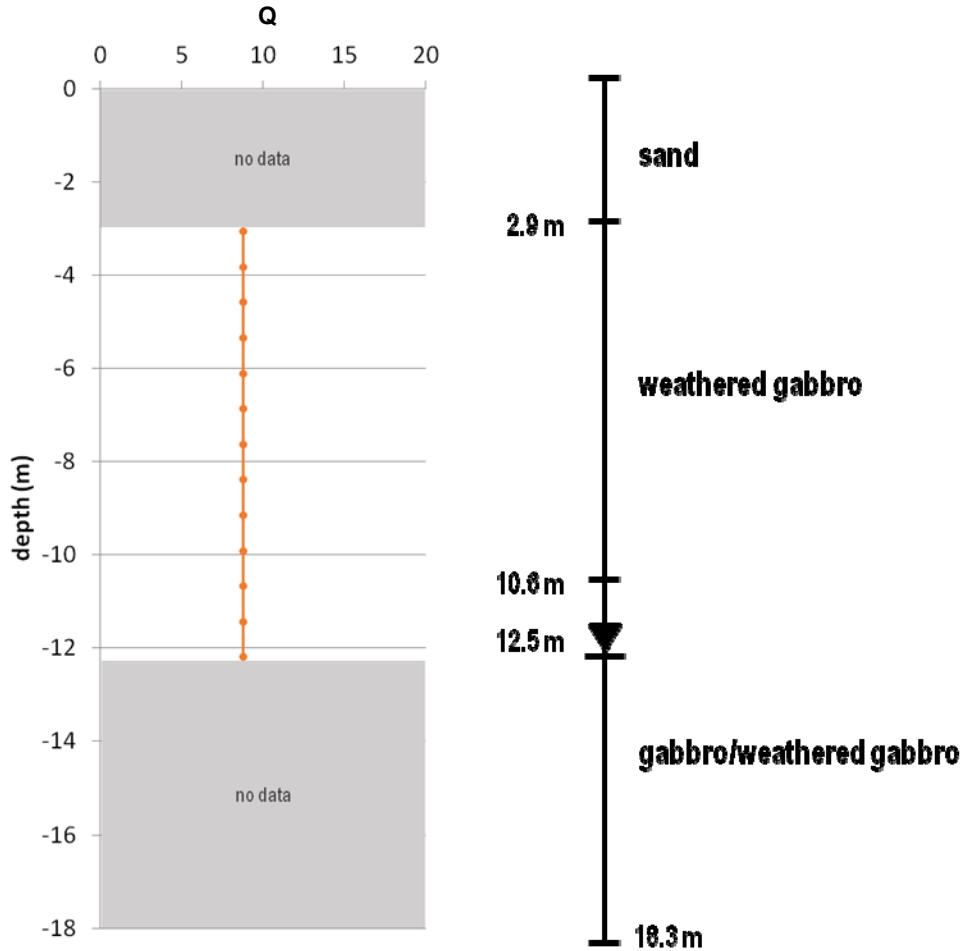
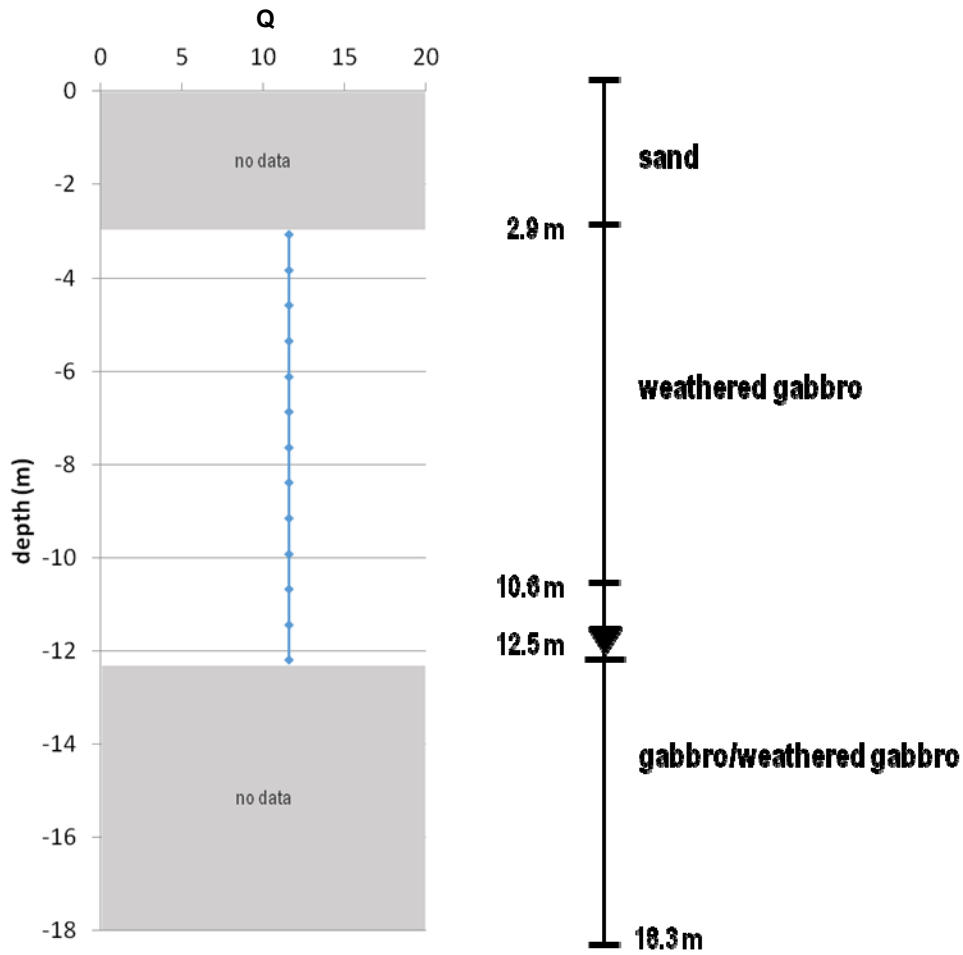


Figure 14: Downhole Qs profile at DTRA-T1.

### Downhole $Q_p$

Bond logs indicate the grout is not well bonded to the formation between receiver depths of 1.5 and 13 m, and the waveforms of direct P-wave recorded within range is inconsistent with deeper receiver stations (Figure 5a). Therefore,  $Q$  estimates for traces within this interval have greater uncertainty. Calculation of  $Q$  is highly sensitive to sources of noise (e.g., traffic) during acquisition.



**Figure 15:** Downhole  $Q_p$  profile at DTRA-T1.

## Surface $Q_s$

Calculation of  $Q$  is highly sensitive to sources of noise (e.g., traffic) during acquisition. Due to lack of stability in the inversion, the upper 10 m is low confidence.

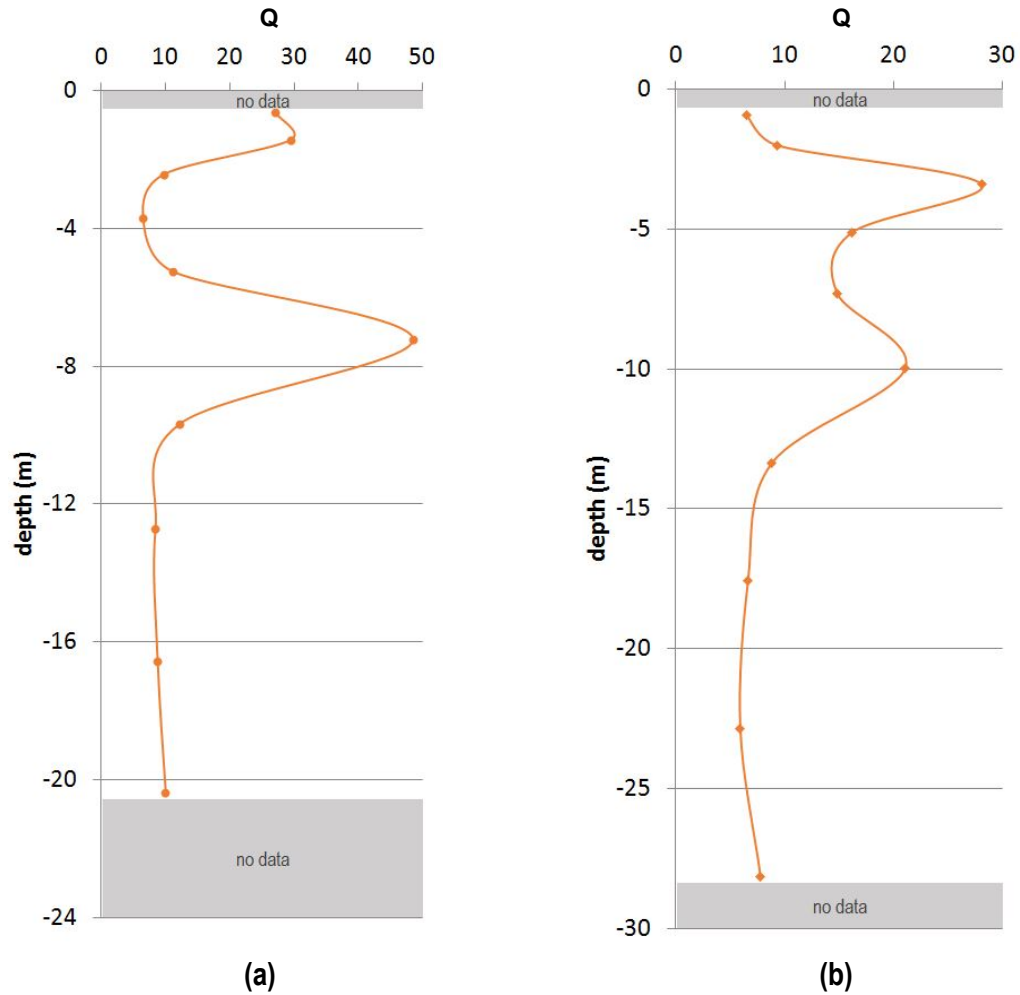


**Figure 16:** Surface  $Q_s$  for lines (a) 1000 and (b) 2000 at DTRA-T1.

## Surface $Q_p$

Calculation of  $Q$  is highly sensitive to sources of noise (e.g., traffic) during acquisition. Due to lack of stability in the inversion, the upper 10 m is low confidence.

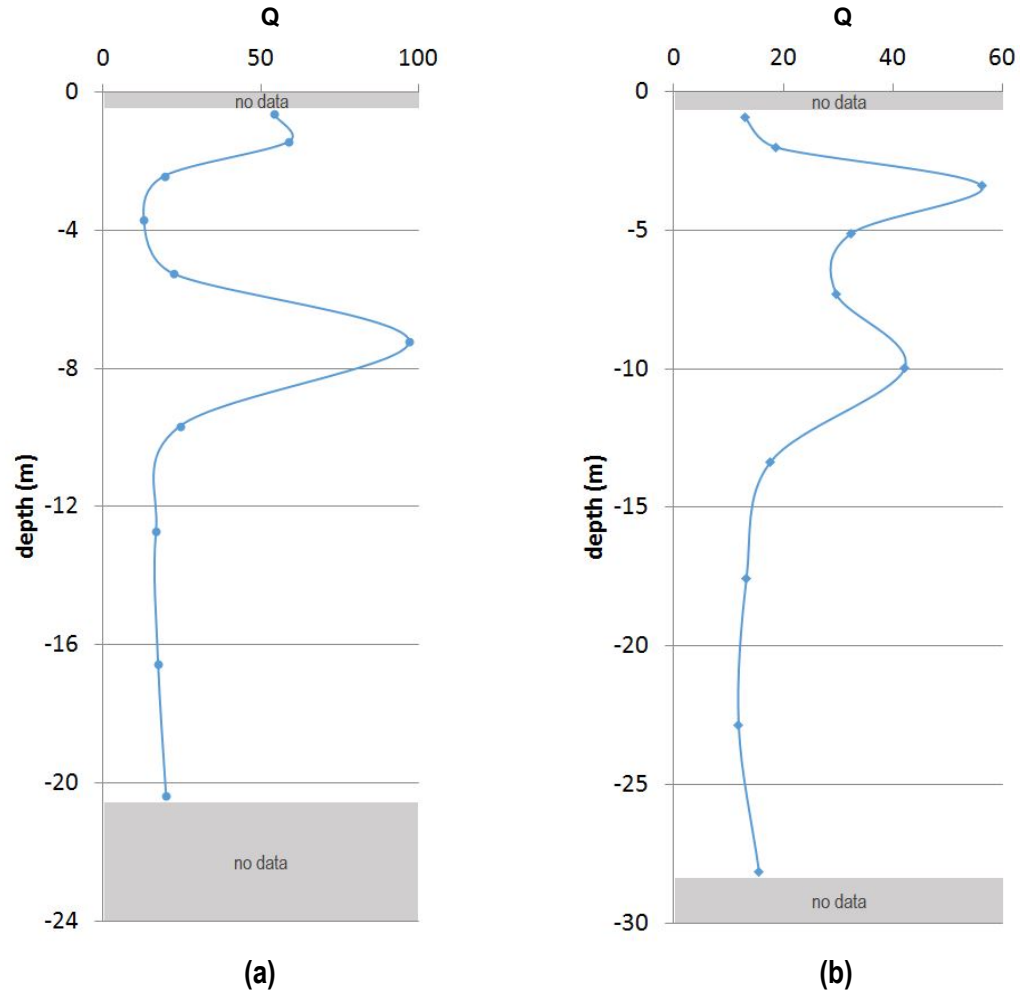


**Figure 17:** Surface  $Q_p$  for lines (a) 1000 and (b) 2000 at DTRA-T1.

## Related Materials

Delivered materials include:

1. This report
2. PowerPoint presentation summarizing this report
3. Data files
4. Document explaining the data file format
5. Detailed list of deliverables

## References

- Di Siena, J.P., J.E. Gaiser, and D. Corrigan, 1984, Horizontal components and shear wave analysis of three component VSP data, in *Vertical Seismic Profiling, Part B: Advanced Concepts*, pp. 175-235, eds. M.N. Toksöz and R.R. Stewart, Geophysical Press, London.
- Hasse, A.B. and R.R. Stewart, 2004, Attenuation estimates from VSP and log data: SEG expanded abstracts, 2497-2500.
- Ivanov, J., R.D. Miller, J. Xia, J.B. Dunbar, and S. Peterie, 2010, Chapter 20: Refraction non-uniqueness studies at levee sites using the refraction-tomography and JARS methods: in *Advances in Near-Surface Seismology and Ground-Penetrating Radar*, SEG Geophysical Developments Series No. 15, R. D. Miller, J. D. Bradford, and K. Holliger, eds., Society of Exploration Geophysicists, 327-338.
- Tonn, R., 1991, The determination of the seismic quality factor Q from VSP data: A comparison of different computational methods: *Geophysical Prospecting*, **39**, 1-27.
- Xia, J., and R.D. Miller, 2010, Chapter 2: Estimation of near-surface shear-wave velocity and quality factor by inversion of high-frequency Rayleigh waves: in *Advances in Near-Surface Seismology and Ground-Penetrating Radar*, SEG Geophysical Developments Series No. 15, R. D. Miller, J. D. Bradford, and K. Holliger, eds., Society of Exploration Geophysicists, 17-36.
- Xia, J., R.D. Miller, and C. B. Park, 1999, Estimation of near-surface velocity by inversion of Rayleigh waves: *Geophysics*, **64**, 691-700.